From Optics, E. Hecht, 3rd ed. (Addison-Wesley, 1998)

directly from the slit to the screen. For the separation a, between the two coherent sources, we take the distance between the actual slit and its image S_1 in the mirror. The spacing of the fringes is once again given by $(s/a)\lambda$. The distinguishing feature of this device is that at glancing incidence ($\theta_i = \pi/2$) the reflected beam undergoes a 180° phase shift. (Recall that the amplitude-reflection coefficients are then both equal to −1). With an additional phase shift of $\pm\pi$,

$$\delta = k(r_1 - r_2) \pm \pi$$

and the irradiance becomes

$$I = 4I_0 \sin^2\left(\frac{\pi a y}{s\lambda}\right)$$

The fringe pattern for Lloyd's mirror is complementary to that of Young's Interferometer; the maxima of one pattern exist at values of y that correspond to minima in the other pattern. The top edge of the mirror is equivalent to $y = 0$ and will be the center of a dark fringe rather than a bright one, as in Young's device. The lower half of the pattern will be obstructed by the presence of the mirror itself. Consider what would happen if a thin sheet of transparent material were placed in the path of the rays traveling directly to the screen. The transparent sheet would have the effect of increasing the number of wavelengths in each direct ray. The entire pattern would accordingly move upward, where the reflected rays would travel a bit farther before interfering. Because of the obvious inherent simplicity of this device, it has been used over a very wide region of the electromagnetic spectrum. The actual reflecting surfaces have ranged from crystals for X-rays, ordinary glass for light, and wire screening for microwaves to a lake or even the Earth's ionosphere for radiowaves.*

All the above interferometers can be demonstrated quite readily either using a laser or, for white light, something a bit more old-fashioned like a discharge lamp or a carbon arc (Fig. 9.15).

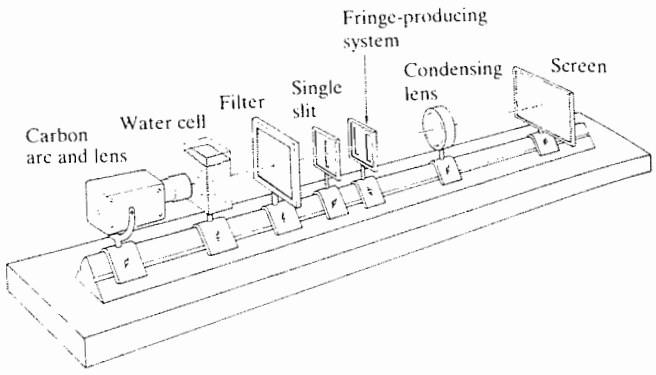

FIGURE 9.15 Bench setup to study wavefront-splitting arrangements with a carbon arc source.The water cell is needed to keep things cool.

9.4 Amplitude-Splitting Interferometers

Suppose that a lightwave is incident on a half-silvered mirror†, or simply on a sheet of glass. Part of the wave is transmitted and part reflected. Both the transmitted and reflected waves have lower amplitudes than the original one. It can be said figuratively that the amplitude has been "split."

If the two separate waves could be brought together again at a detector, interference would result, as long as the original coherence between the two had not been destroyed. If the path lengths differed by a distance greater than that of the wavegroup (i.e., the coherence length), the portions reunited at the detector would correspond to different wavegroups. No unique phase relationship would exist between them in that case, and the fringe pattern would be unstable to the point of being unobservable. We will get back to these ideas when we consider coherence theory in more detail. For the moment the discussion is restricted, for the most part, to those cases for which the path difference is less than the coherence length.

*For a discussion of the effects of a finite slit width and a finite frequency bandwidth, see R. N. Wolfe and F. C. Eisen, "Irradiance Distribution in a Lloyd Mirror Interference Pattern," *J. Opt. Soc. Am.* **38**, 706 (1948).

†A *half-silvered mirror* is one that is semitransparent, because the metallic coating is too thin to be opaque. You can look through it, and at the same time you can see your reflection in it. *Beamsplitters*, as devices of this kind are called, can also be made of thin stretched plastic films, known as *pellicles*, or even uncoated glass plate.

9.4.1 Dielectric Films—Double-Beam Interference

Interference effects are observable in sheet transparent materials, the thicknesses of which vary over a very broad range, from films less than the length of a lightwave (e.g., for green light λ_0 equals about $\frac{1}{150}$ the thickness of this printed page) to plates several centimeters thick. A layer of material is referred to as a *thin film* for a given wavelength of electromagnetic radiation when its thickness is of the order of that wavelength. Before the early 1940s interference phenomena associated with thin dielectric films, although well known, had fairly limited practical value. The rather spectacular color displays arising from oil slicks and soap films, however pleasing aesthetically and theoretically, were mainly curiosities.

With the advent of suitable vacuum deposition techniques in the 1930s, precisely controlled coatings could be produced on a commercial scale, and that, in turn, led to a rebirth of interest in dielectric films. During the Second World War, both sides were finding the enemy with a variety of coated optical devices, and by the 1960s multilayered coatings were in widespread use.

Fringes of Equal Inclination

Consider the simple case of a transparent parallel plate of dielectric material having a thickness d (Fig. 9.16). Suppose that the film is nonabsorbing and that the amplitude-reflection coefficients at the interfaces are so low that only the first two reflected beams E_{1r} and E_{2r} (both having undergone only one reflection) need be considered (Fig. 9.17). In practice, the amplitudes of the higher-order reflected beams (E_{3r}, etc.) generally decrease very rapidly, as can be shown for the air–water and air–glass interfaces (Problem 9.23). For the moment, consider S to be a monochromatic point source.

The film serves as an amplitude-splitting device, so that E_{1r} and E_{2r} may be considered as arising from two coherent virtual sources lying behind the film; that is, the two images of S formed by reflection at the first and second interfaces. The reflected rays are parallel on leaving the film and can be brought together at a point P on the focal plane of a telescope objective or on the retina of the eye when focused at infinity. From Fig. 9.17, the optical path length difference for the first two reflected beams is given by

$$\Lambda = n_f[(\overline{AB}) + (\overline{BC})] - n_1(\overline{AD})$$

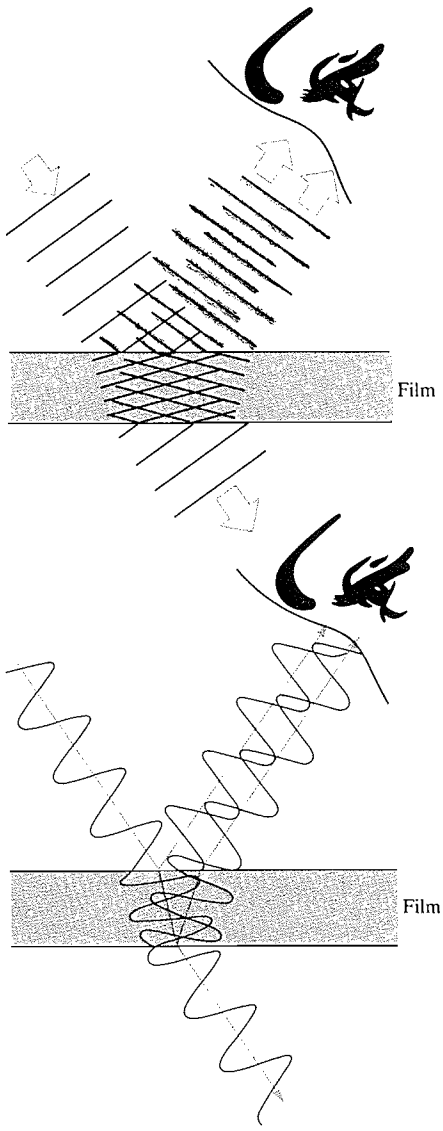

FIGURE 9.16 The wave and ray representations of thin-film interference. Light reflected from the top and bottom of the film interferes to create a fringe pattern.

and since $(\overline{AB}) = (\overline{BC}) = d/\cos\theta_t$,

$$\Lambda = \frac{2n_f d}{\cos\theta_t} - n_1(\overline{AD})$$

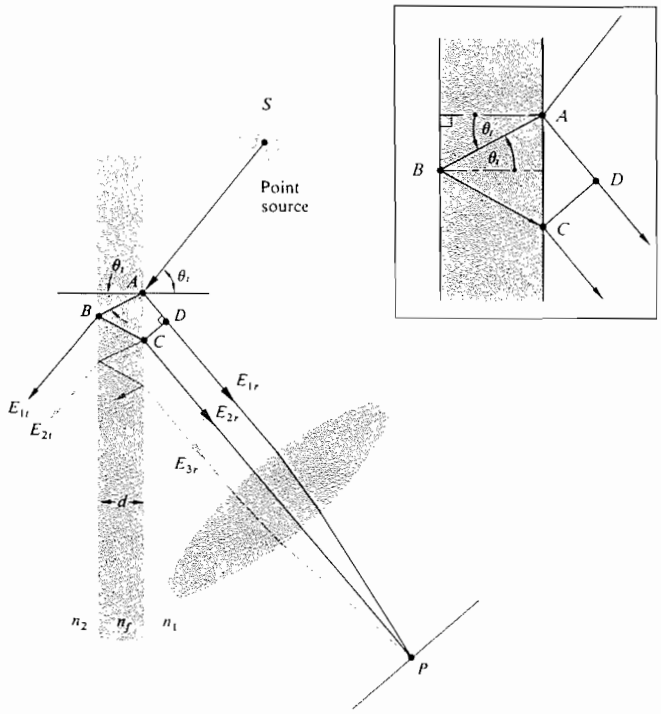

FIGURE 9.17 Fringes of equal inclination.

Now, to find an expression for $(\overline{AD})$, write

$$(\overline{AD}) = (\overline{AC}) \sin \theta_i$$

Using Snell's Law, this becomes

$$(\overline{AD}) = (\overline{AC}) \frac{n_f}{n_1} \sin \theta_t$$

where

$$(\overline{AC}) = 2d \tan \theta_t \tag{9.32}$$

The expression for Λ now becomes

$$\Lambda = \frac{2n_f d}{\cos \theta_t} (1 - \sin^2 \theta_t)$$

or finally

$$\Lambda = 2n_f d \cos \theta_t \tag{9.33}$$

The corresponding phase difference associated with the optical path length difference is then just the product of the free-space propagation number and Λ, that is, $k_0\Lambda$. If the film is immersed in a single medium, the index of refraction can simply be written as $n_1 = n_2 = n$. Realize that n may be less than n_f, as in the case of a soap film in air, or greater than n_f, as with an air film between two sheets of glass. In either case *there will be an additional phase shift arising from the reflections themselves*. Recall that for incident angles up to about 30°, regardless of the polarization of the incoming light, the two beams, one internally and one externally reflected, will experience a *relative phase shift* of π radians (Fig. 4.43 and Section 4.3). Accordingly,

$$\delta = k_0\Lambda \pm \pi$$

and more explicitly

$$\delta = \frac{4\pi n_f}{\lambda_0} d \cos \theta_t \pm \pi \tag{9.34}$$

or

$$\delta = \frac{4\pi d}{\lambda_0} (n_f^2 - n^2 \sin^2 \theta_i)^{1/2} \pm \pi \tag{9.35}$$

The sign of the phase shift is immaterial, so we will choose the negative sign to make the equations a bit simpler. In reflected

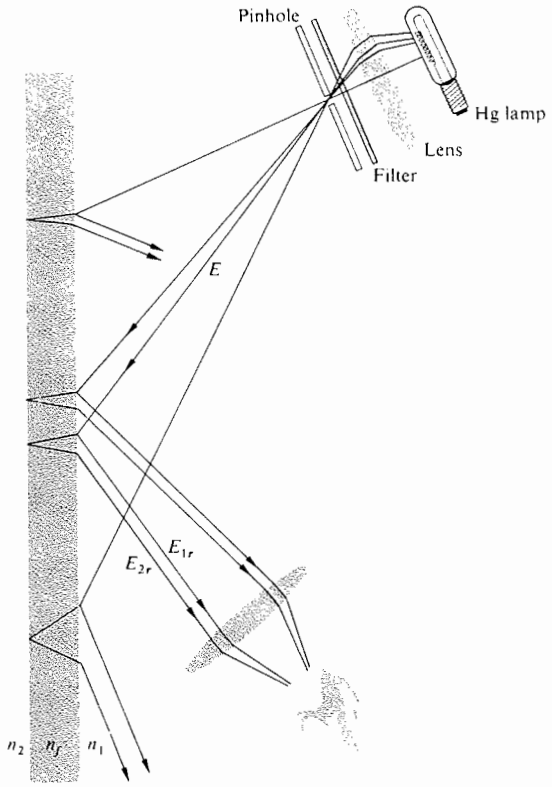

FIGURE 9.18 Fringes seen on a small portion of the film.

light an interference maximum, a bright spot, appears at P when $\delta = 2m\pi$—in other words, an even multiple of π. In that case Eq. (9.34) can be rearranged to yield

[maxima] $$d \cos \theta_t = (2m + 1)\frac{\lambda_f}{4} \qquad m = 0,1,2,\ldots \tag{9.36}$$

where use has been made of the fact that $\lambda_f = \lambda_0/n_f$. This also corresponds to minima in the transmitted light. Interference minima in reflected light (maxima in transmitted light) result when $\delta = (2m \pm 1)\pi$, that is, odd multiples of π. For such cases Eq. (9.34) yields

[minima] $$d \cos \theta_t = 2m\frac{\lambda_f}{4} \tag{9.37}$$

The appearance of odd and even multiples of $\lambda_f/4$ in Eqs. (9.36) and (9.37) is significant , as we will see presently. We could, of course, have a situation in which $n_1 > n_f > n_2$ or $n_1 < n_f < n_2$, as with a fluoride film deposited on an optical element of glass immersed in air. The π phase shift would then not be present, and the above equations would simply be modified appropriately.

If the lens used to focus the rays has a small aperture, interference fringes will appear on a small portion of the film. Only the rays leaving the point source that are reflected directly into the lens will be seen (Fig. 9.18). For an extended source, light will reach the lens from various directions, and the fringe pattern will spread out over a large area of the film (Fig. 9.19).

The angle θ_i or equivalently θ_t, determined by the position of P, will in turn control δ. The fringes appearing at points P_1 and P_2 in Fig. 9.20 are known as **fringes of equal inclination**. (Problem 9.28 discusses some easy ways to see these fringes.) Keep in mind that each source point on the extended source is incoherent with respect to the others. When the image of the extended source is reflected in the surface, it will be seen to be banded with bright and dark fringes. Each of these is an arc of a circle centered on the intersection of a perpendicular dropped from the eye to the film.

As the film becomes thicker, the separation $\overline{AC}$ between E_{1r} and E_{2r} also increases, since

$$\overline{AC} = 2d \tan \theta_t \tag{9.32}$$

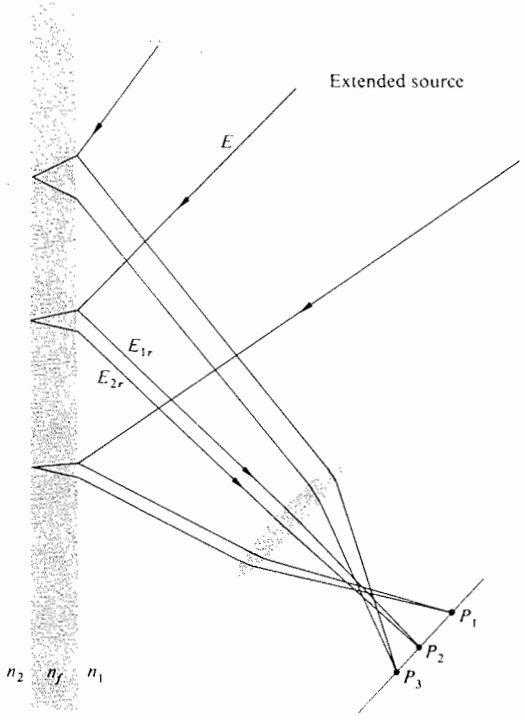

FIGURE 9.19 Fringes seen on a large region of the film.

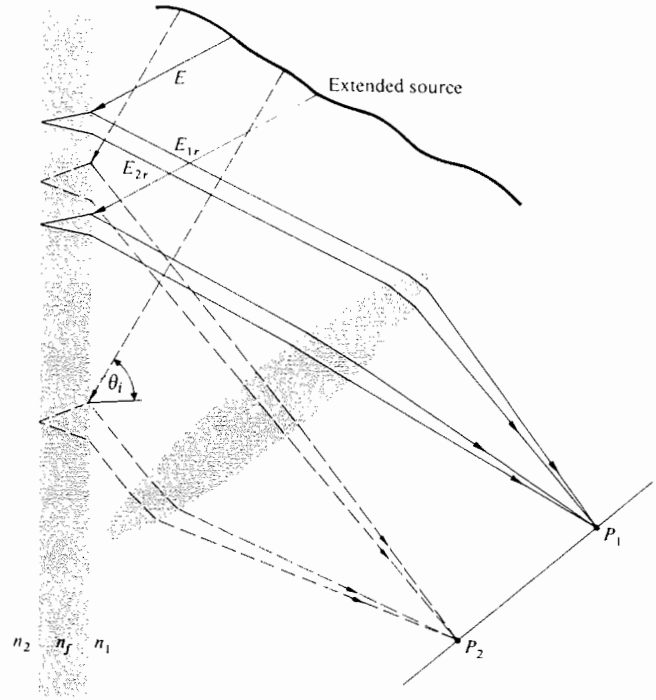

FIGURE 9.20 All rays inclined at the same angle arrive at the same point.

When only one of the two rays is able to enter the pupil of the eye, the interference pattern will disappear. The larger lens of a telescope can then be used to gather in both rays, once again making the pattern visible. The separation can also be reduced by reducing θ_t and therefore θ_i, that is, by viewing the film at nearly normal incidence. The equal-inclination fringes that are seen in this manner for thick plates are known as **Haidinger fringes**, after the Austrian physicist Wilhelm Karl Haidinger (1795–1871). With an extended source, the symmetry of the setup requires that the interference pattern consists of a series of concentric circular bands centered on the perpendicular drawn from the eye to the film (Fig. 9.21). As the observer moves, the interference pattern follows along.

Haidinger fringes can be seen in the ordinary window glass of a store front. Find one with a neon sign in the window and look out at the street, at night, very close to the glowing tube. You'll see circular fringes centered on your eye floating off in the distance.

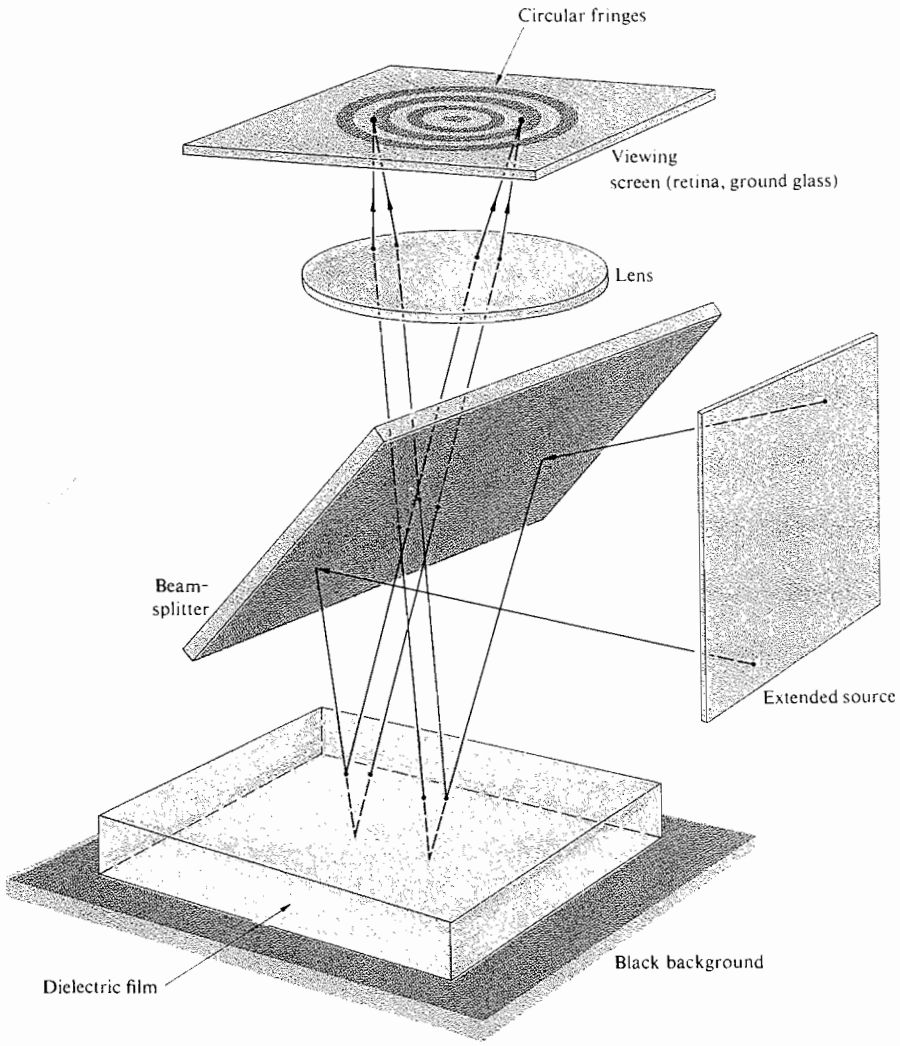

FIGURE 9.21 Circular Haidinger fringes centered on the lens axis.

Fringes of Equal Thickness

A whole class of interference fringes exists for which the optical thickness, $n_f d$, is the dominant parameter rather than θ_i. These are referred to as **fringes of equal thickness**. Under white-light illumination the iridescence of soap bubbles, oil slicks (a few wavelengths thick), and even oxidized metal surfaces is the result of variations in film thickness. Interference bands of this kind are analogous to the constant-height contour lines of a topographical map. Each fringe is the locus of all points in the film for which the optical thickness is a constant. In general, n_f does not vary, so that the fringes correspond to regions of constant film thickness. As such, they can be quite useful in determining the surface features of optical elements (lenses, prisms, etc.). For example, a surface to be examined may be put into contact with an *optical flat*.* The air in the space between the two generates a thin-film interference pattern. If the test surface is flat, a series of straight, equally spaced bands indicates a wedge-shaped air film, usually resulting from dust between the flats. Two pieces of plate glass separated at one end by a strip of paper will form a satisfactory wedge with which to observe these bands.

When viewed at nearly normal incidence in the manner illustrated in Fig. 9.22, the contours arising from a nonuniform film are called **Fizeau fringes**. For a thin wedge of small angle α, the optical path length difference between two reflected rays may be approximated by Eq. (9.33), where d is the thickness at a particular point, that is,

$$d = x\alpha \tag{9.38}$$

For small values of θ_i the condition for an interference maximum becomes

$$(m + \tfrac{1}{2})\lambda_0 = 2n_f d_m$$

or

$$(m + \tfrac{1}{2})\lambda_0 = 2\alpha x_m n_f$$

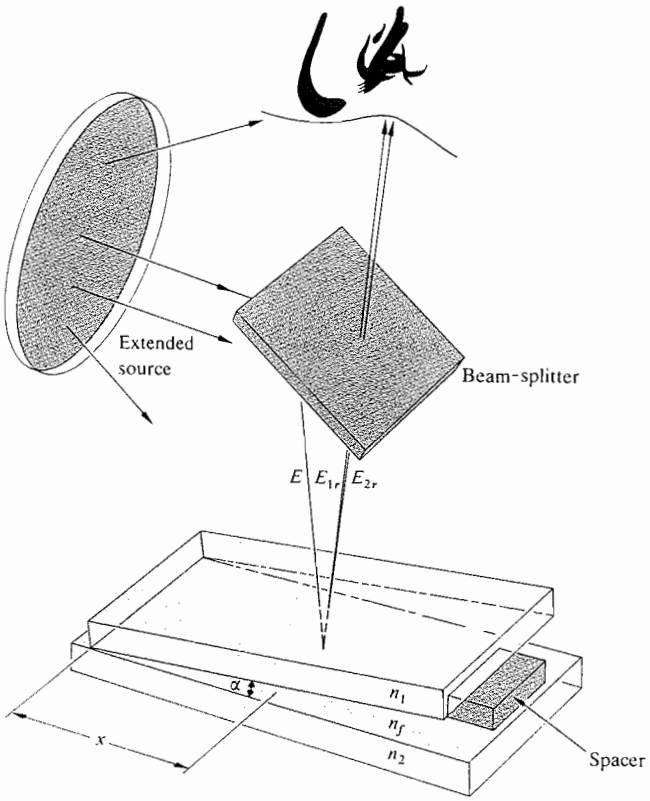

FIGURE 9.22 Fringes from a wedge-shaped film.

Since $n_f = \lambda_0/\lambda_f$, x_m may be written as

$$x_m = \left(\frac{m + 1/2}{2\alpha}\right)\lambda_f \tag{9.39}$$

Maxima occur at distances from the apex given by $\lambda_f/4\alpha$, $3\lambda_f/4\alpha$, and so on, and consecutive fringes are separated by a distance Δx, given by

$$\Delta x = \lambda_f/2\alpha \tag{9.40}$$

Notice that the difference in film thickness between adjacent maxima is simply $\lambda_f/2$. Since the beam reflected from the lower surface traverses the film twice ($\theta_i \approx \theta_t \approx 0$), adjacent maxima differ in optical path length by λ_f. Note, too, that the film thickness at the various maxima is given by

$$d_m = (m + \tfrac{1}{2})\frac{\lambda_f}{2} \tag{9.41}$$

*A surface is said to be optically flat when it deviates by not more than about $\lambda/4$ from a perfect plane. In the past, the best flats were made of clear fused quartz. Now glass-ceramic materials (e.g., CERVIT) having extremely small thermal coefficients of expansion (about one-sixth that of quartz) are available. Individual flats of $\lambda/200$ or a bit better can be made.

which is an odd multiple of a quarter wavelength. Traversing the film twice yields a phase shift of π, which when added to the shift of π resulting from reflection, puts the two rays back in-phase.

Figure 9.23 is a photograph of a soap film held vertically so that it settles into a wedge shape under the influence of gravity. When illuminated with white light, the bands are various colors. The black region at the top is a portion where the film is less than $\lambda_f/4$ thick. Twice this, plus an additional shift of $\lambda_f/2$ due to the reflection, is less than a whole wavelength. The reflected rays are therefore out-of-phase. As the thickness decreases still further, the total phase difference approaches π. The irradiance at the observer goes to a minimum (Eq. 9.16), and the film appears black in reflected light.*

Press two well-cleaned microscope slides together. The enclosed air film will usually not be uniform. In ordinary room light a series of irregular, colored bands (fringes of equal thickness) will be clearly visible across the surface (Fig. 9.24). The thin glass slides distort under pressure, and the fringes move and change accordingly. Tape two slides together with transparent (matt-surfaced) tape. It will scatter light and make the reflected fringes more easily seen.

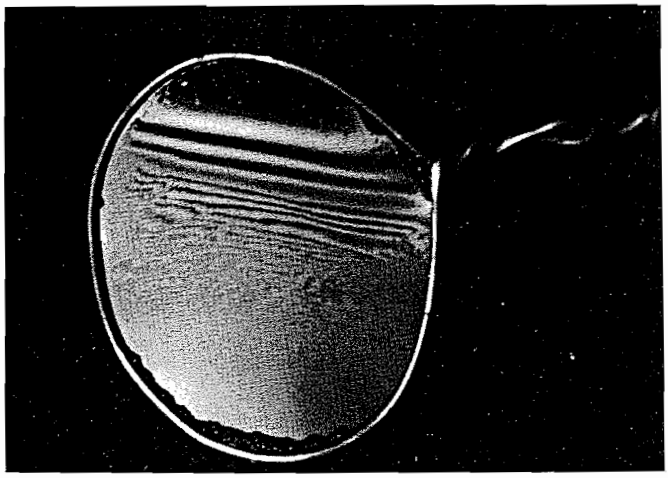

FIGURE 9.23 A wedge-shaped film made of liquid dishwashing soap. (E. H.)

*The relative phase shift of π between internal and external reflection is required if the reflected flux density is to go to zero smoothly, as the film gets thinner and finally disappears.

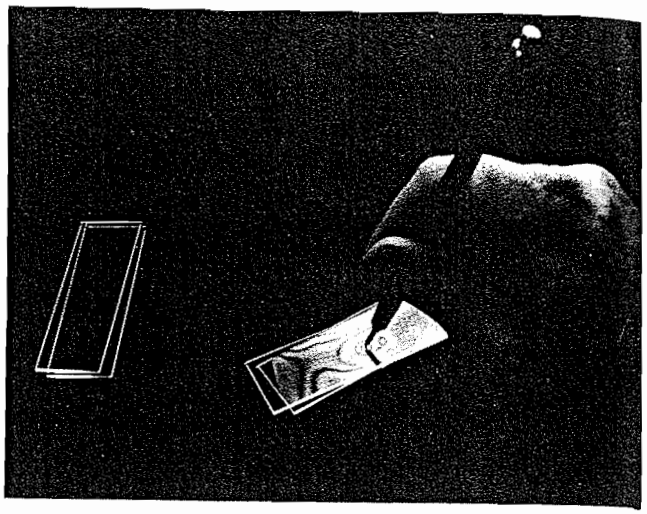

(a)

FIGURE 9.24 Fringes created by an air film between two microscope slides. (Photo by E. H.)

If the two pieces of glass are forced together at a point, as might be done by pressing on them with a sharp pencil, a series of concentric, nearly circular, fringes is formed about that point. Known as **Newton's rings*** (Fig. 9.25), this pattern is more precisely examined with the arrangement of Fig. 9.26. Here a lens is placed on an optical flat and illuminated at normal incidence with quasimonochromatic light. The amount of uniformity in the concentric circular pattern is a measure of the degree of perfection in the shape of the lens. With R as the radius of curvature of the convex lens, the relation between the distance x and the film thickness d is given by

$$x^2 = R^2 - (R - d)^2$$

or more simply by

$$x^2 = 2Rd - d^2$$

*Robert Hooke (1635–1703) and Isaac Newton independently studied a whole range of thin-film phenomena, from soap bubbles to the air film between lenses. Quoting from Newton's *Opticks*:

> I took two Object-glasses, the one a Planoconvex for a fourteen Foot Telescope, and the other a large double Convex for one of about fifty Foot; and upon this, laying the other with its plane side downwards, I pressed them slowly together to make the Colours successfully emerge in the middle of the Circles.

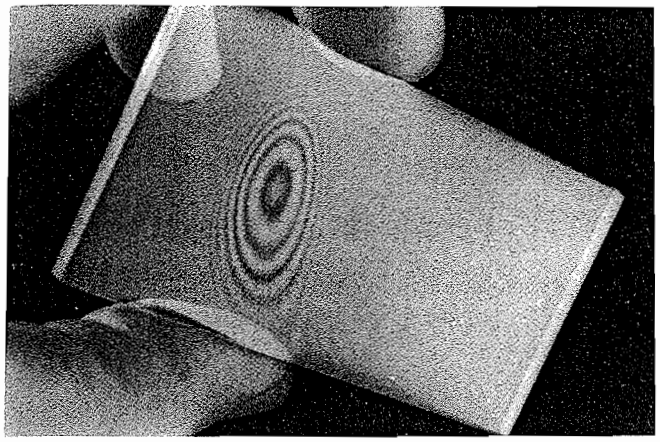

FIGURE 9.25 Newton's rings with two microscope slides. (E. H.)

Since $R >> d$, this becomes

$$x^2 = 2Rd$$

Assume that we need only examine the first two reflected beams E_{1r} and E_{2r}. The mth-order interference maximum will occur in the thin film when its thickness is in accord with the relationship

$$2n_f d_m = (m + \tfrac{1}{2})\lambda_0$$

The radius of the mth bright ring is therefore found by combining the last two expressions to yield

[bright ring] $$x_m = [(m + \tfrac{1}{2})\lambda_f R]^{1/2} \tag{9.42}$$

Similarly, the radius of the mth dark ring is

[dark ring] $$x_m = (m\lambda_f R)^{1/2} \tag{9.43}$$

If the two pieces of glass are in good contact (no dust), the central fringe at that point ($x_0 = 0$) will clearly be a minimum in irradiance, an understandable result since d goes to zero at that point. In transmitted light, the observed pattern will be the complement of the reflected one discussed above, so that the center will now appear bright.

Newton's rings, which are Fizeau fringes, can be distinguished from the circular pattern of Haidinger's fringes by the manner in which the diameters of the rings vary with the order m. The central region in the Haidinger pattern corresponds to the maximum value of m (Problem 9.27), whereas just the opposite applies to Newton's rings.

An optical shop, in the business of making lenses, will have a set of precision spherical test plates or gauges. A designer can specify the surface accuracy of a new lens in terms of the number and regularity of the Newton rings that will be seen with a particular test gauge. The use of test plates in the manufacture of high-quality lenses, however, is giving way to far more sophisticated techniques involving laser interferometers (Section 9.8.2).

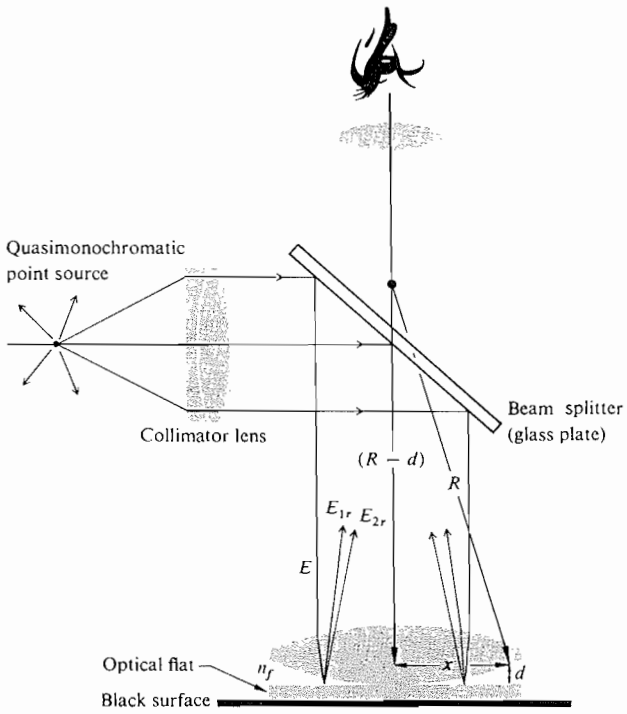

FIGURE 9.26 A standard setup to observe Newton's rings.

9.4.2 Mirrored Interferometers

There are a good number of amplitude-splitting interferometers that utilize arrangements of mirrors and beamsplitters. By far the best known and historically the most important of these is the **Michelson Interferometer**. Its configuration is illustrated in Fig. 9.27. An extended source (e.g., a diffusing ground-glass plate illuminated by a discharge lamp) emits a wave, part of which travels to the right. The beamsplitter at O divides the wave into two, one segment traveling to the right

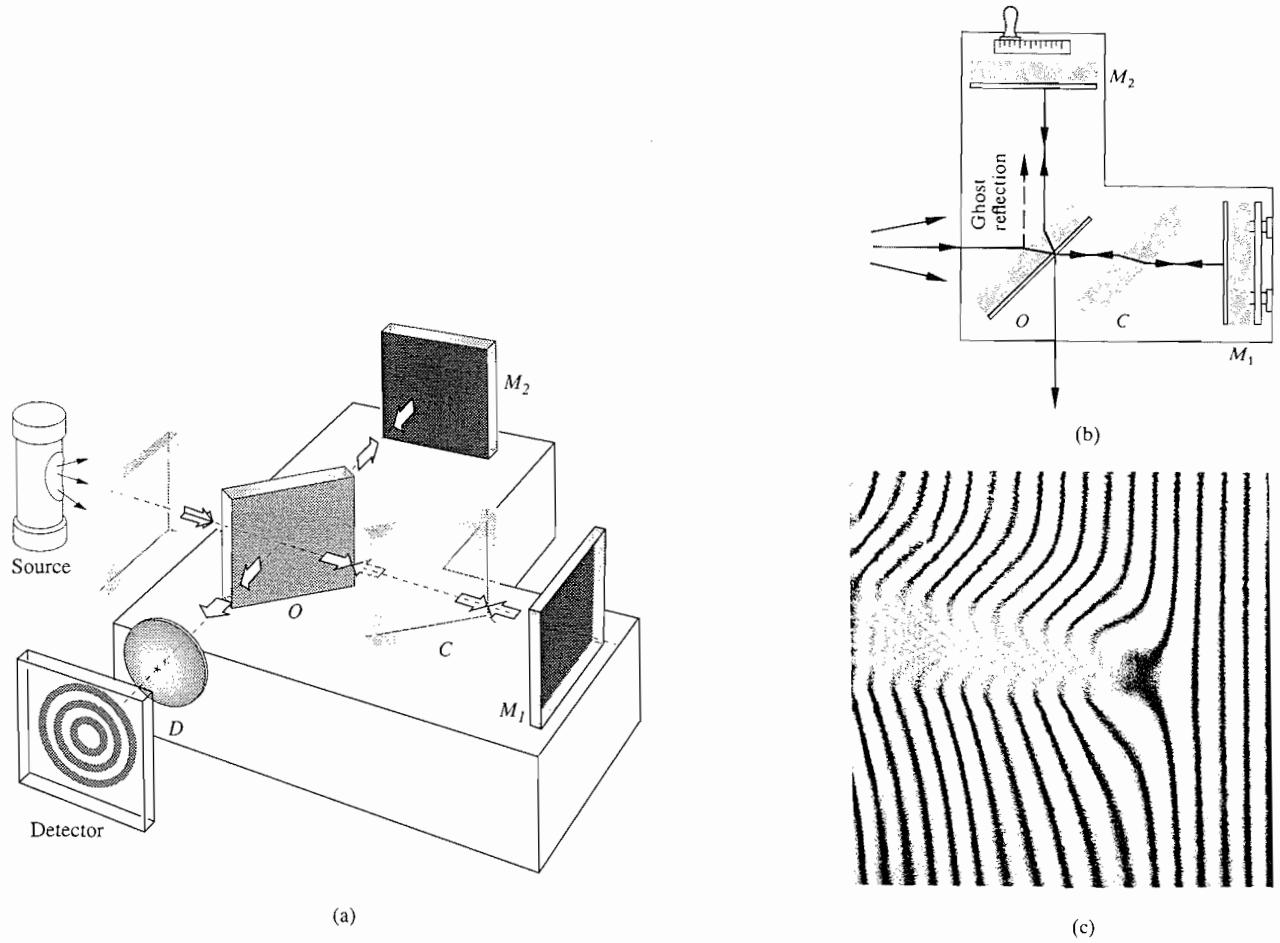

FIGURE 9.27 The Michelson Interferometer. (*a*) Circular fringes are centered on the lens. (*b*) Top view of the interferometer showing the path of the light. (*c*) A wedge fringe pattern was distorted when the tip of a hot soldering iron was placed in one arm. Observe the interesting perceptual phenomenon whereby the region corresponding to the iron's tip appears faintly yellow. (E. H.)

and one up into the background. The two waves are reflected by mirrors M_1 and M_2 and return to the beamsplitter. Part of the wave coming from M_2 passes through the beamsplitter going downward, and part of the wave coming from M_1 is deflected by the beamsplitter toward the detector. The two waves are united, and interference can be expected.

Notice that one beam passes through O three times, whereas the other traverses it only once. Consequently, each beam will pass through equal thicknesses of glass only when a *compensator plate* C is inserted in the arm OM_1. The compensator is an exact duplicate of the beamsplitter, with the exception of any possible silvering or thin film coating on the beamsplitter. It is positioned at an angle of 45°, so that O and C are parallel to each other. With the compensator in place, any optical path difference arises from the actual path difference. In addition, because of the dispersion of the beamsplitter, the optical path is a function of λ. Accordingly, for quantitative work, the interferometer without the compensator plate can be used only with a quasimonochromatic source. The inclusion of a compensator negates the effect of dispersion, so that even a source with a very broad bandwidth will generate discernible fringes.

To understand how fringes are formed, refer to the construction shown in Fig. 9.28, where the physical components are represented more as mathematical surfaces. An observer at the position of the detector will simultaneously see both mirrors M_1 and M_2 along with the source Σ in the beamsplitter. We can redraw the interferometer as if all the elements were in a straight line. Here M_1' corresponds to the image of mirror M_1 in the beamsplitter, and Σ has been swung over in line with O and M_2. The positions of these elements in the diagram depend on their relative distances from O (e.g., M_1' can be in front of, behind, or coincident with M_2 and can even pass through it). The surfaces Σ_1 and Σ_2 are the images of the source Σ in mirrors M_1 and M_2, respectively. Now consider a single point S on the source emitting light in all directions; let's follow the course of one emerging ray. In actuality a wave from S will be split at O, and its segments will thereafter be reflected by M_1 and M_2. In our schematic diagram we represent this by reflecting the ray off both M_2 and M_1'. To an observer at D, the two reflected rays will appear to have come from the image points S_1 and S_2 [note that all rays shown in (a) and (b) of Fig. 9.28 share a common plane-of-incidence]. For all practical purposes, S_1 and S_2 are coherent point sources, and we can anticipate a flux-density distribution obeying Eq. (9.14).

As the figure shows, the optical path difference for these rays is nearly $2d \cos \theta$, which represents a phase difference of $k_0 2d \cos \theta$. There is an additional phase term arising from the fact that the wave traversing the arm OM_2 is internally reflected in the beamsplitter, whereas the OM_1-wave is externally reflected at O. If the beamsplitter is simply an uncoated glass plate, the relative phase shift resulting from the two reflections

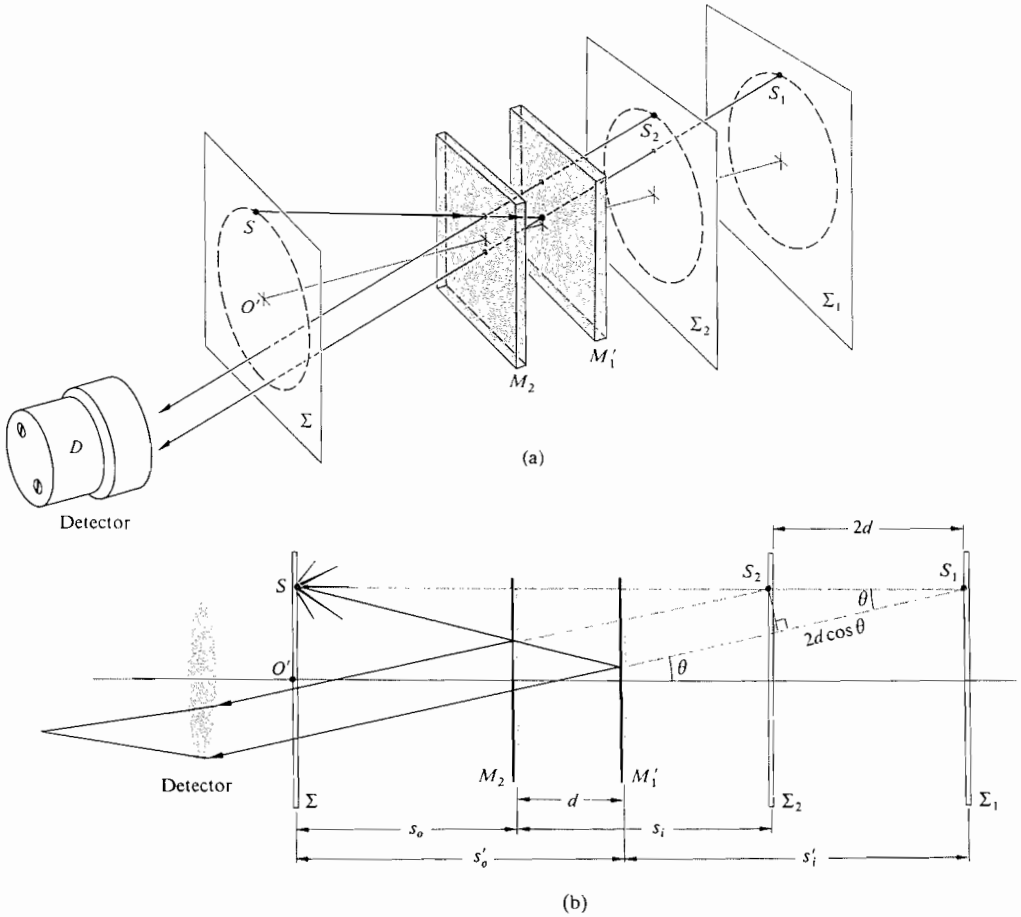

FIGURE 9.28 A conceptual rearrangement of the Michelson Interferometer.

will be π radians. *Destructive*, rather than constructive, interference will then exist when

$$2d \cos \theta_m = m\lambda_0 \tag{9.44}$$

where m is an integer. If this condition is fulfilled for the point S, then it will be equally well fulfilled for any point on Σ that lies on the circle of radius $O'S$, where O' is located on the axis of the detector. As illustrated in Fig. 9.29, an observer will see a circular fringe system concentric with the central axis of her eye's lens. Because of the small aperture of the eye, the observer will not be able to see the entire pattern without the use of a large lens near the beamsplitter to collect most of the emergent light.

If we use a source containing a number of frequency components (e.g., a mercury discharge lamp), the dependence of θ_m on λ_0 in Eq. (9.44) requires that each such component generate a fringe system of its own. Note, too, that since $2d \cos \theta_m$ must be less than the coherence length of the source, it follows that laser light will be particularly easy to use in demonstrating the interferometer (see Section 9.5). This point would be made strikingly evident were we to compare the fringes produced by laser light with those generated by "white" light from an ordinary tungsten bulb or a candle. In the latter case, the path difference must be very nearly zero, if we are to see any fringes at all, whereas in the former instance a difference of 10 cm has little noticeable effect.

An interference pattern in quasimonochromatic light typically consists of a large number of alternatively bright and dark rings. A particular ring corresponds to a fixed *order m*. As M_2 is moved toward M_1', d decreases, and according to Eq. (9.44), cos θ_m increases while θ_m therefore decreases. The rings shrink toward the center, with the highest-order one disappearing whenever d decreases by $\lambda_0/2$. Each remaining ring broadens as more and more fringes vanish at the center, until only a few fill the whole screen. By the time $d = 0$ has been reached, the central fringe will have spread out, filling the entire field of view. With a phase shift of π resulting from reflection off the beamsplitter, the whole screen will then be an interference minimum. (Lack of perfection in the optical elements can render this unobservable.) Moving M_2 still farther causes the fringes to reappear at the center and move outward.

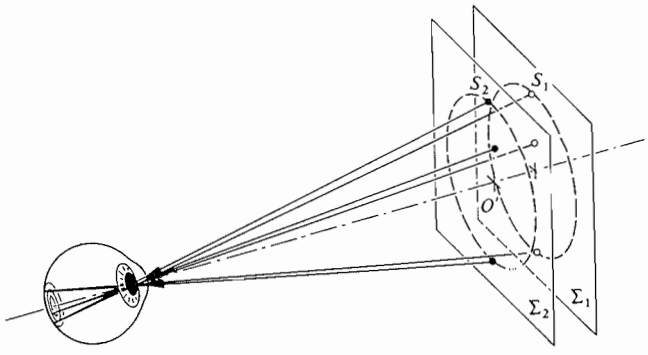

FIGURE 9.29 Formation of circular fringes.

Notice that a central dark fringe for which $\theta_m = 0$ in Eq. (9.44) can be represented by

$$2d = m_0\lambda_0 \tag{9.45}$$

(Keep in mind that this is a special case. The central region might correspond to neither a maximum nor a minimum.) Even if d is 10 cm, which is fairly modest in laser light, and $\lambda_0 = 500$ nm, m_0 will be quite large, namely 400 000. At a fixed value of d, successive dark rings will satisfy the expressions

$$\begin{aligned} 2d \cos \theta_1 &= (m_0 - 1)\lambda_0 \\ 2d \cos \theta_2 &= (m_0 - 2)\lambda_0 \\ &\vdots \\ 2d \cos \theta_p &= (m_0 - p)\lambda_0 \end{aligned} \tag{9.46}$$

The angular position of any ring, for example, the pth ring, is determined by combining Eqs. (9.45) and (9.46) to yield

$$2d(1 - \cos \theta_p) = p\lambda_0 \tag{9.47}$$

Since $\theta_m \equiv \theta_p$, both are just the half-angle subtended at the detector by the particular ring, and since $m = m_0 - p$, Eq. (9.47) is equivalent to Eq. (9.44). The new form is somewhat more convenient, since (using the same example as above) with $d = 10$ cm, the sixth dark ring can be specified by stating that $p = 6$, or in terms of the *order* of the pth ring, that $m = 399\,994$. If θ_p is small,

$$\cos \theta_p = 1 - \frac{\theta_p^2}{2}$$

and Eq. (9.47) yields

$$\theta_p = \left(\frac{p\lambda_0}{d}\right)^{1/2} \tag{9.48}$$

for the angular radius of the pth fringe.

The construction of Fig. 9.28 represents one possible configuration, the one in which we consider only pairs of parallel emerging rays. Since these rays do not actually meet, they cannot form an image without a condensing lens of some sort. Indeed, that lens is most often provided by the observer's eye focused at infinity. The resulting *fringes of equal inclination* (θ_m = constant) located at infinity are also *Haidinger fringes*. A comparison of Figs. 9.28*b* and 9.3*a*, both showing two coherent point sources, suggests that in addition to these (virtual) fringes at infinity, there might also be (real) fringes formed by converging rays. These fringes do in fact exist. Hence, if you illuminate the interferometer with a *broad source* and shield out all extraneous light, you can easily see the projected pattern on a screen in a darkened room (see Section 9.5). The fringes will appear in the space in front of the interferometer (i.e., where the detector is shown), and their size will increase with increasing distance from the beamsplitter. We will consider the (real) fringes arising from point-source illumination a little later on.

When the mirrors of the interferometer are inclined with respect to each other, making a small angle (i.e., when M_1 and M_2 are not quite perpendicular), *Fizeau fringes* are observed. The resultant wedge-shaped air film between M_2 and M_1' creates a pattern of straight parallel fringes. The interfering rays appear to diverge from a point behind the mirrors. The eye would have to focus on this point in order to make these *localized fringes* observable. It can be shown analytically* that by appropriate adjustment of the orientation of the mirrors M_1 and M_2, fringes can be produced that are straight, circular, elliptical, parabolic, or hyperbolic—this holds as well for the real and virtual fringes.

The Michelson Interferometer can be used to make extremely accurate length measurements. As the moveable mirror is displaced by $\lambda_0/2$, each fringe will move to the position previously occupied by an adjacent fringe. Using a microscope arrangement, one need only count the number of fringes N, or portions thereof, that have moved past a reference point to determine the distance traveled by the mirror Δd, that is,

$$\Delta d = N(\lambda_0/2)$$

Nowadays this can be done fairly easily by electronic means. Michelson used the method to measure the number of wavelengths of the red cadmium line corresponding to the standard meter in Sévres near Paris.†

The Michelson Interferometer can be used along with a few polaroid filters to verify the Fresnel–Arago Laws. A polarizer inserted in each arm will allow the optical path length difference to remain fairly constant, while the vector field directions of the two beams are easily changed.

A microwave Michelson Interferometer can be constructed with sheet-metal mirrors and a chicken-wire beamsplitter. With the detector located at the central fringe, it can easily measure shifts from maxima to minima as one of the mirrors is moved, thereby determining λ. A few sheets of plywood, plastic, or glass inserted in one arm will change the central fringe. Counting the number of fringe shifts yields a value for the index of refraction, and from that we can compute the dielectric constant of the material.

The **Mach–Zehnder Interferometer** is another amplitude-splitting device. As shown in Fig. 9.30, it consists of two beamsplitters and two totally reflecting mirrors. The two waves within the apparatus travel along separate paths. A difference between the optical paths can be introduced by a slight tilt of one of the beamsplitters. Since the two paths are separated, the interferometer is relatively difficult to align. For the

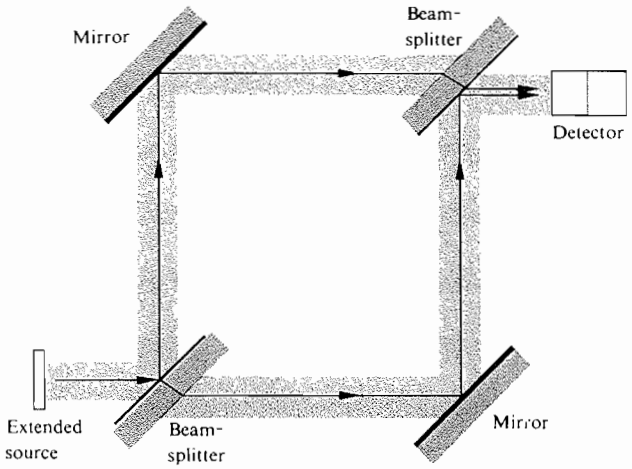

FIGURE 9.30 The Mach–Zehnder Interferometer.

*See, for example, Valasek, *Optics*, p. 135.

†A discussion of the procedure he used to avoid counting the 3 106 327 fringes directly can be found in Strong, *Concepts of Classical Optics*, p. 238, or Williams, *Applications of Interferometry*, p. 51.

same reason, however, the interferometer finds myriad applications. It has even been used, in a somewhat altered yet conceptually similar form, to obtain electron interference fringes.*

An object interposed in one beam will alter the optical path length difference, thereby changing the fringe pattern. A common application of the device is to observe the density variations in gas-flow patterns within research chambers (wind tunnels, shock tubes, etc.). One beam passes through the optically flat windows of the test chamber, while the other beam traverses appropriate compensator plates. The beam within the chamber will propagate through regions having a spatially varying index of refraction. The resulting distortions in the wavefront generate the fringe contours. A particularly nice application is shown in Fig. 9.31, which is a photograph of the magnetic compression device known as Scylla IV. It was used to study controlled thermonuclear reactions at the Los Alamos Scientific Laboratory. In this application, the Mach–Zehnder Interferometer appears in the form of a parallelogram, as illustrated in Fig. 9.32. The two ruby laser *interferograms*, as these photographs are called, show (Fig. 9.33) the background pattern without a plasma in the tube and the density contours within the plasma during a reaction (Fig. 9.34).

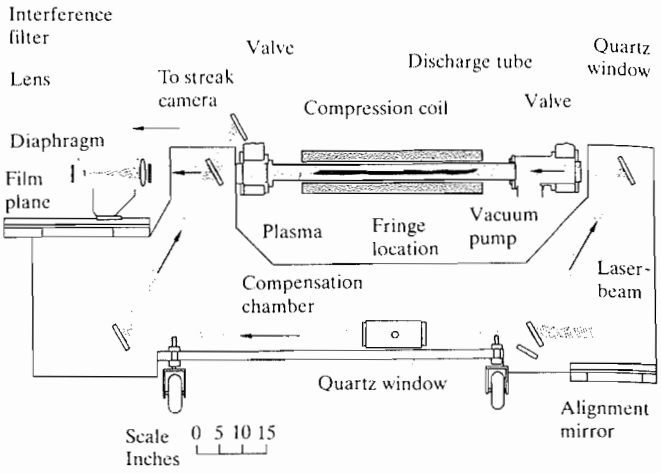

FIGURE 9.32 Schematic of Scylla IV.

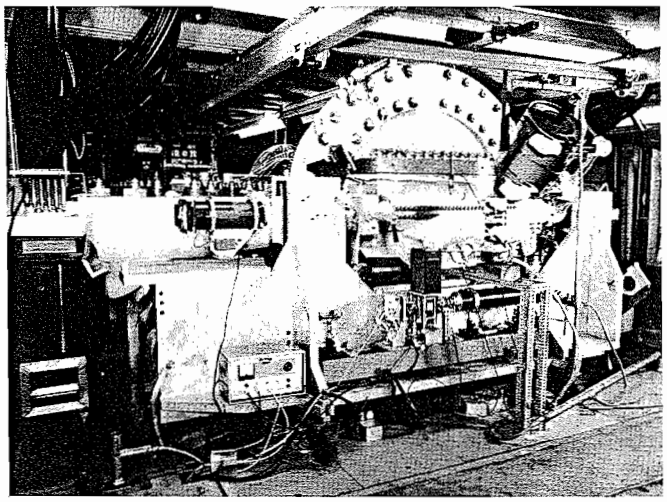

FIGURE 9.31 Scylla IV (Courtesy of University of California, Lawrence Livermore National Laboratory, and the Department of Energy)

Another amplitude-splitting device, which differs from the previous instrument in many respects, is the **Sagnac Interferometer**. It is very easy to align and quite stable. An interesting application of the device is discussed in the last section of this chapter, where we consider its use as a gyroscope. One form

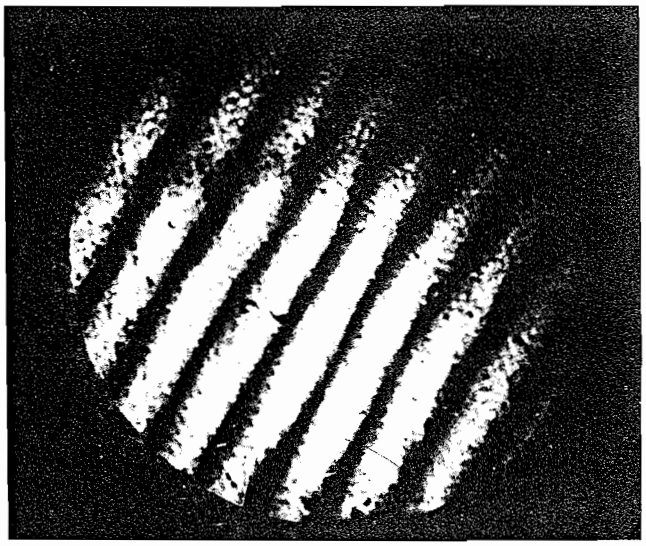

FIGURE 9.33 Interferogram without plasma. (Photo courtesy Los Alamos National Laboratory.)

*L. Marton, J. Arol Simpson, and J. A. Suddeth, *Rev. Sci. Instr.* **25**, 1099 (1954), and *Phys. Rev.* **90**, 490 (1953).

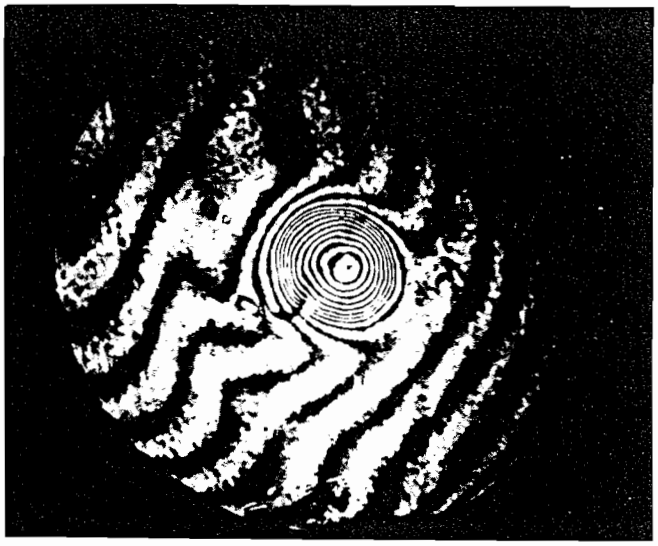

FIGURE 9.34 Interferogram with plasma. (Photo courtesy Los Alamos National Laboratory.)

of the Sagnac Interferometer is shown in Fig. 9.35*a* and another in Fig. 9.35*b*; still others are possible. Notice that the main feature of the device is that there are two identical but oppositely directed paths taken by the beams and that both form closed loops before they are united to produce interference. A deliberate slight shift in the orientation of one of the mirrors will produce a path length difference and a resulting fringe pattern. Since the beams are superimposed and therefore inseparable, the interferometer cannot be put to any of the conventional uses. These in general depend on the possibility of imposing variations on only one of the constituent beams.

Real Fringes

Before we examine the creation of real, as opposed to virtual, fringes, let's first consider another amplitude-splitting interferometric device, the **Pohl fringe-producing system**, illustrated in Fig. 9.36. It is simply a thin transparent film illuminated by the light coming from a point source. In this case, the fringes are real and can accordingly be intercepted on a screen placed anywhere in the vicinity of the interferometer without a condensing-lens system. A convenient light source to use is a mercury lamp covered with a shield having a small hole ($\approx\frac{1}{4}$ inch diameter) in it. As a thin film, use a piece of ordinary mica taped to a dark-colored book cover, which serves as an opaque backing. If you have a laser, its remarkable coherence length and high flux density will allow you to perform this same experiment with almost anything smooth and transparent. Expand the beam to about an inch or two in diameter by passing it through a lens (a focal length of 50 to 100 mm will do). Then just reflect the beam off the surface of a glass plate (e.g., a microscope slide), and the fringes will be

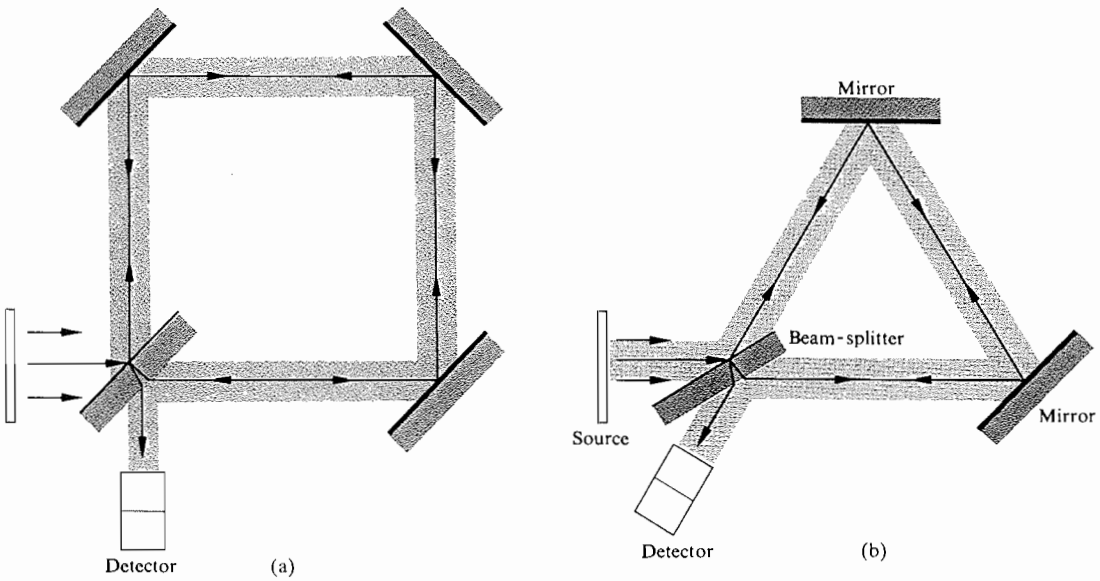

FIGURE 9.35 (*a*) A Sagnac Interferometer. (*b*) Another variation of the Sagnac Interferometer.

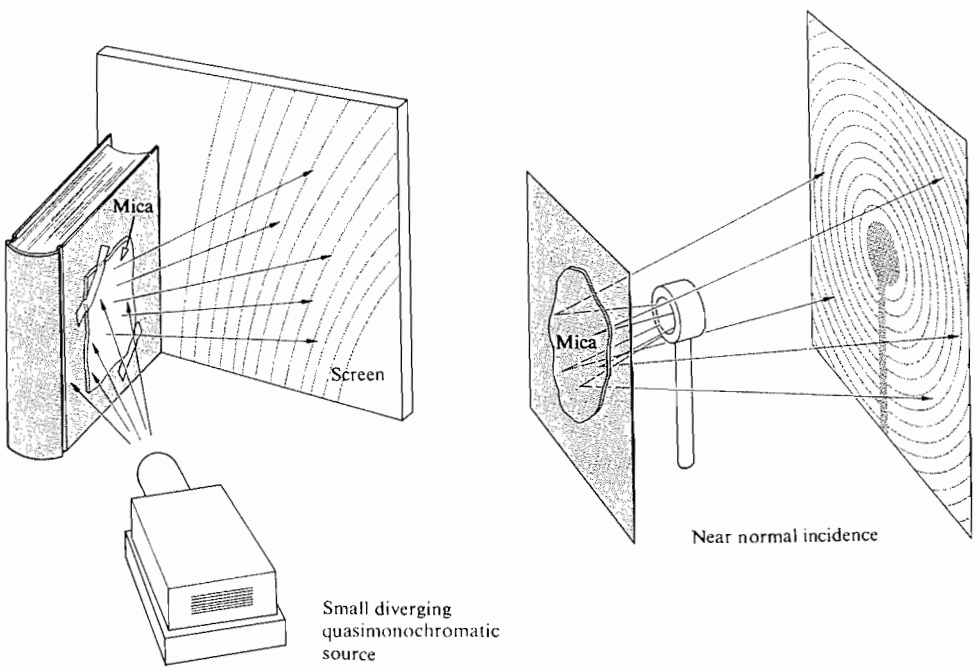

FIGURE 9.36 The Pohl Interferometer.

evident within the illuminated disk wherever it strikes a screen.

The underlying physical principle involved with point-source illumination for all four of the interferometric devices considered above can be appreciated with the help of a construction, variations of which are shown in Figs. 9.37 and 9.38.* The two vertical lines in Fig. 9.37, or the inclined ones in Fig. 9.38, represent either the positions of the mirrors or the two sides of the thin sheet in the Pohl Interferometer. Let's assume that point P in the surrounding medium is a point at which there is constructive interference. A screen placed at that point would intercept this maximum, as well as a whole fringe pattern, without any condensing system. The coherent virtual sources emitting the interfering beams are mirror images S_1 and S_2 of the actual point source S. It should be noted that this kind of real fringe pattern can be observed with both the Michelson and Sagnac Interferometers (Fig. 9.39). If either

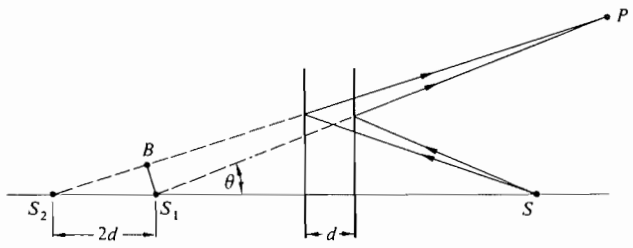

FIGURE 9.37 Point-source illumination of parallel surfaces.

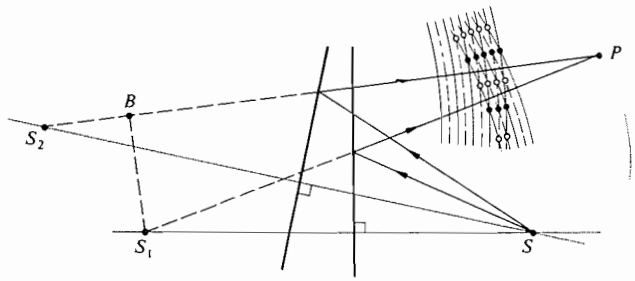

FIGURE 9.38 Point-source illumination of inclined surfaces.

*A. Zajac, H. Sadowski, and S. Licht, "The Real Fringes in the Sagnac and the Michelson Interferometers," *Am. J. Phys.* **29**, 669 (1961).

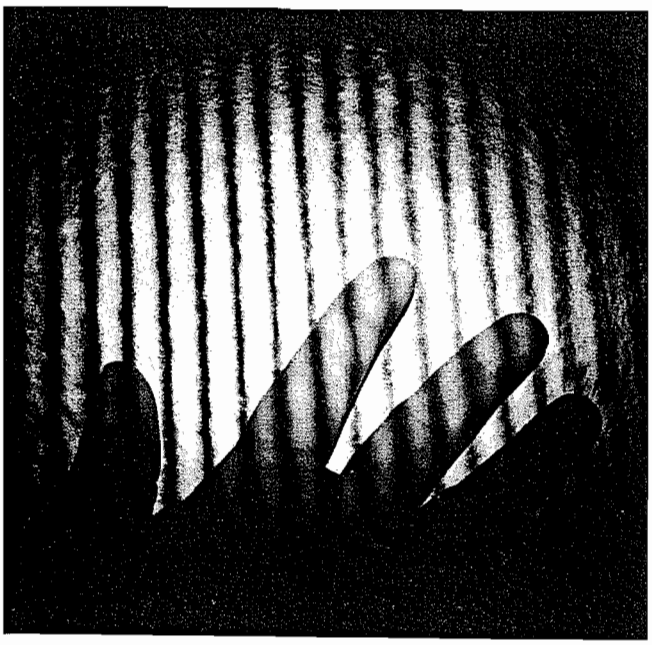

FIGURE 9.39 Real Michelson fringes using He–Ne laser light. (E. H.)

device is illuminated with an expanded laserbeam, a real fringe pattern will be generated directly by the emerging waves. This is an extremely simple and beautiful demonstration.

9.5 Types and Localization of Interference Fringes

Often it is important to know where the fringes produced in a given interferometric system will be located, since that is the region where we need to focus our detector (eye, camera, telescope). In general, the problem of locating fringes is characteristic of a given interferometer; that is, it has to be solved for each individual device.

Fringes can be classified, first, as either *real* or *virtual* and, second, as either *nonlocalized* or *localized*. Real fringes are those that can be seen on a screen without the use of an additional focusing system. The rays forming these fringes converge to the point of observation, all by themselves. Virtual fringes cannot be projected onto a screen without a focusing system. In this case the rays obviously do not converge.

Nonlocalized fringes are real and exist everywhere within an extended (three-dimensional) region of space. The pattern is literally nonlocalized, in that it is not restricted to some small region. Young's Experiment, as illustrated in Fig. 9.8, fills the space beyond the secondary sources with a whole array of real fringes. Nonlocalized fringes of this sort are generally produced by small sources, that is, point or line sources, be they real or virtual. In contrast, localized fringes are clearly observable only over a particular surface. The pattern is literally localized, whether near a thin film or at infinity. This type of fringe will always result from the use of extended sources but can be generated with a point source as well.

The Pohl Interferometer (Fig. 9.36) is particularly useful in illustrating these principles, since with a point source it will produce both real nonlocalized and virtual localized fringes. The real nonlocalized fringes (Fig. 9.40, upper half) can be intercepted on a screen almost anywhere in front of the mica film.

For the nonconverging rays, realize that since the aperture of the eye is quite small, it will intercept only those rays that are directed almost exactly at it. For this small pencil of rays, the eye, at a particular position, sees either a bright or dark spot but not much more. To perceive an extended fringe pattern formed by parallel rays of the type shown in the bottom half of Fig. 9.40, a large lens will have to be used to gather in light entering at other orientations. In practice, however, the source is usually somewhat extended, and fringes can generally be seen by looking into the film with the eye focused at infinity. These virtual fringes are localized at infinity and are equivalent to the *equal-inclination fringes* of Section 9.4. Similarly, if the mirrors M_1 and M_2 in the Michelson Interferometer are parallel, the usual circular, virtual, equal-inclination fringes localized at infinity will be seen. We can imagine a thin air film between the surfaces of the mirrors M_2 and M_1' acting to generate these fringes. As with the configuration of Fig. 9.40 for the Pohl device, real nonlocalized fringes will also be present.

The geometry of the fringe pattern seen in reflected light from a transparent wedge of small angle α is shown in Fig. 9.41. The fringe location P will be determined by the direction of incidence of the incoming light. Newton's rings have this same kind of localization, as do the Michelson, Sagnac, and other interferometers for which the equivalent interference

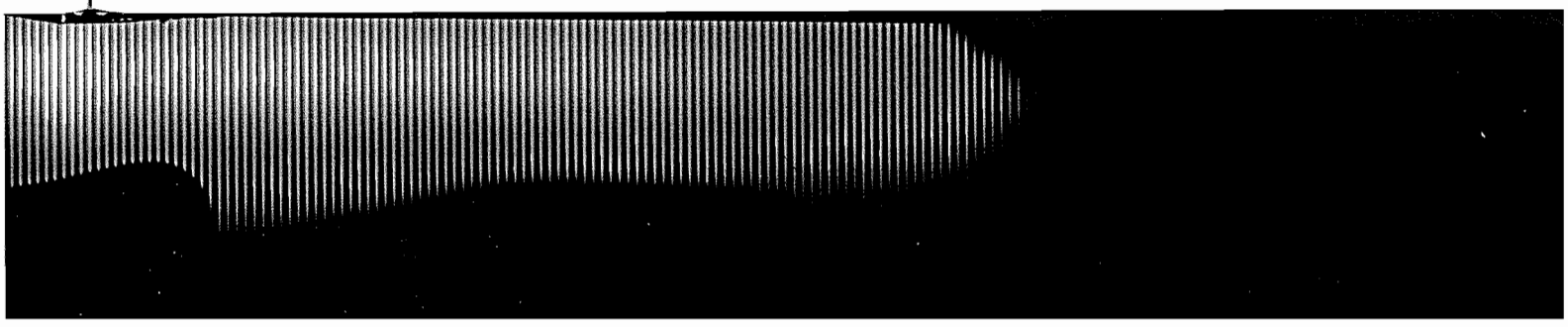

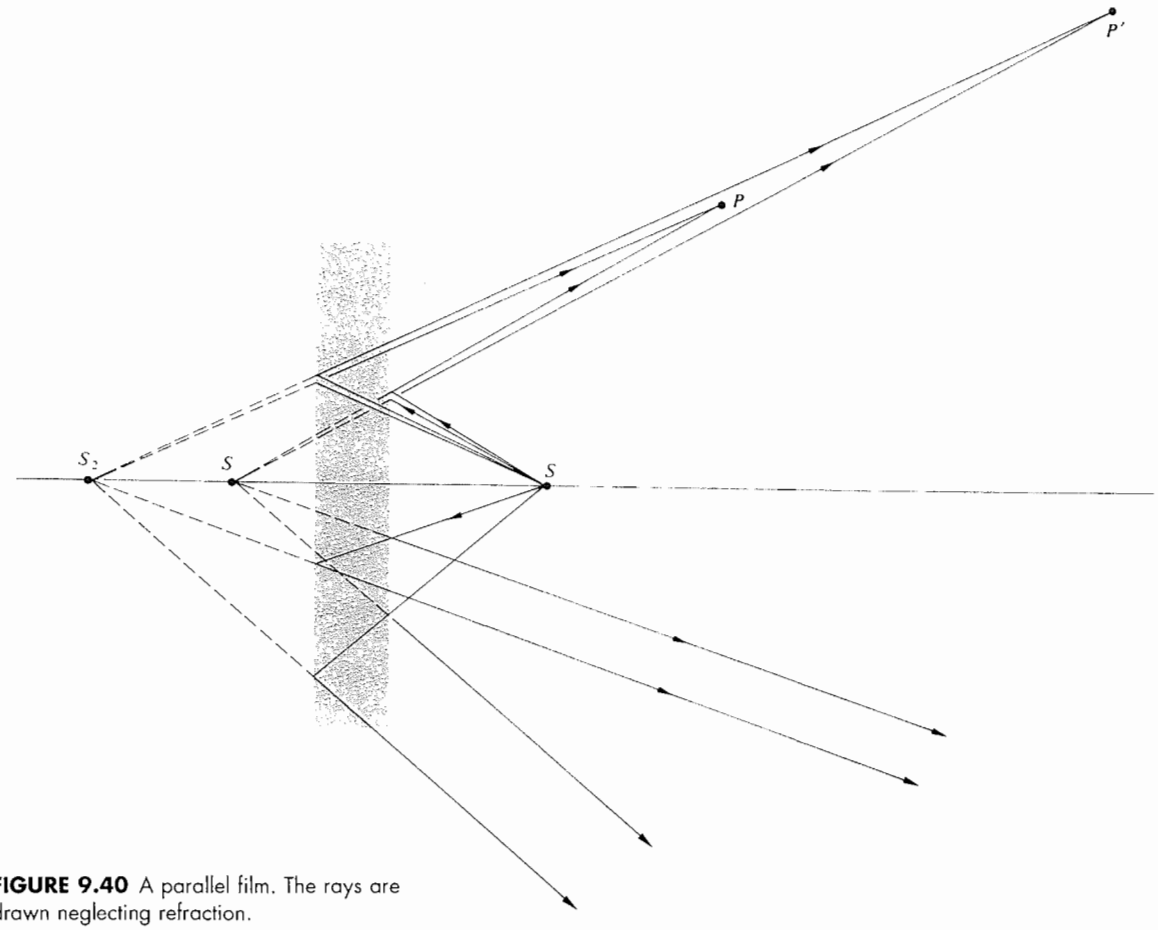

FIGURE 9.40 A parallel film. The rays are drawn neglecting refraction.

system consists of two reflecting planes inclined slightly to each other. The wedge setup of the Mach–Zehnder Interferometer is distinctive in that by rotating the mirrors, one can localize the resulting virtual fringes on any plane within the region generally occupied by the test chamber (Fig. 9.42).

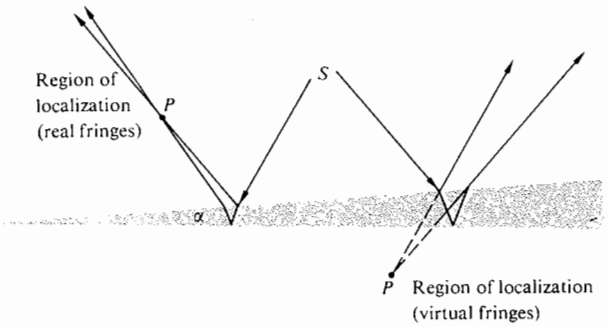

FIGURE 9.41 Fringes formed by a wedge-shaped film.

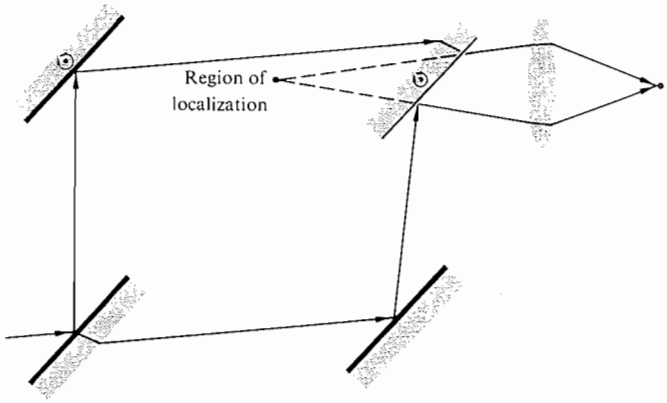

FIGURE 9.42 Fringes in the Mach–Zehnder Interferometer.